CORE2018 CONFERENCE ON RAILWAY EXCELLENCE
Rail: smart, automated, sustainable RTSA

Material characteristics of laser-cladded hypereutectoid rail steels

Q. Lai[1], T. Roy[1], R. Abrahams[1], W. Yan[1], A. Paradowska[2], C. Qiu[3], P. Mutton[3], and M. Soodi[4]

[1]Department of Mechanical & Aerospace Engineering, Monash University, Clayton VIC 3800, Australia

[2]Australian Nuclear Science & Technology Organization, Lucas Heights NSW 2234, Australia

[3]Institute of Railway Technology, Monash University, Clayton VIC 3800, Australia

[4]Hardchrome Engineering, Clayton VIC 3168, Australia

Corresponding Author: quan.lai@monash.edu

SUMMARY

The impact of preheating conditions and carbon dilution on the microstructural and mechanical properties of laser cladded rails at various number of deposition layers has been investigated for a hypereutectoid steel grades typically used under heavy haul conditions. The microstructures in the HAZ showed that formation of martensite, which has a detrimental effect on behaviour in wheel-rail contact, was successfully inhibited by increasing the length of the preheated region using a preheating temperature of 350 °C. Dilution of carbon from the hypereutectoid substrate was observed and its effect on the microstructures of the 410L ferritic stainless-steel deposits was investigated. The formation of ferrite in the 410L cladding layers was attributed to the very low carbon content, and no carbide formation was observed on boundaries of the ferritic grains. The thickness of dilution band was determined to be approximately equal to the thickness of the first cladding layer. Mechanical characterization of the 410L deposits undertaken in terms of Vickers microhardness was correlated with the observed microstructural morphologies.

1. INTRODUCTION

Material degradation in the form of wear and rolling contact fatigue (RCF) in the rail head is induced by the complex contact between wheels and rails. Remedial actions such as rail grinding or wheel machining, and eventually component substitution, contribute a significant part of the cost of railway network operation. Regular maintenance or even replacement of the damaged components can also lead to disruptions in rail haulage operations, and adverse economic impacts.

Application of surface engineering techniques, i.e. laser glazing and laser cladding, either to repair existing damage or during manufacture, have been attempted to extend component service lives and maintenance intervals, while conserving the properties of the parent rails. Previous studies [1-3] addressing the localized damage on railhead surfaces by the utilization of the laser surface treatments, particularly laser cladding technique, have demonstrated encouraging results and promising potential as techniques for alleviating the rate of component degradation.

Briefly, laser cladding process is a melting process in which a focused laser beam is utilized to deposit a coating of the selected material onto the target surfaces. Dimelfi et al.[1] and Aldajah et al.[2] performed laser glazing of a pearlitic rail substrate and obtained reductions in the surface friction coefficient and lateral forces, respectively. Shariff et al.[3] investigated the effects of laser hardening and laser melting on wear performance of the T-12 Indian rail steel and reported that the friction coefficient was marginally deducted. Niederhauser et al.[4] examined the mechanical properties of the B-82 Swedish rail steel cladded with Co-Cr alloys and showed a consistent and promising fatigue performance. Ringsberg et al. [5] performed finite element analysis on the European pearlitic UIC 900A (R260) steel cladded with Co-Cr alloys and found that the laser cladding and grinding processes decreased the safety margin against fatigue failure. Franklin et al.[6] validated Ringsberg et al.'s FEA results by conducting laboratory experiments of cladded R260 rail samples under simulated wheel-rail contact conditions. A laser cladded (InfraStar) rail materials survived 200,000 cycles of water-lubricated twin-disc testing without crack formation, whereas UIC (260 grade) 900A base material showed severe cracking after only 4000 cycles. Furthermore, the cladded rails with the InfraStar materials were field tested by Hiensch et al.[7] and showed no RCF damage over one year in track where the non-treated rail showed clear RCF damage.

The previous studies were performed using eutectoid carbon rail steel grades. Of interest in the current investigation is the influence of the higher carbon levels associated with premium rail grades such as those used under heavy haul conditions on the characteristics of the cladding layers and the heat-affected zone. For such an application, information on two fundamental issues, i.e. effects of the higher carbon levels on the characteristics of the cladding layers, and martensitic formation in

Effects of preheating and carbon dilution on material characteristics of laser-cladded hypereutectoid rail steels

Q. Lai[1], T. Roy[1], R. Abrahams[1], W. Yan[1], A. Paradowska[2], C. Qiu[3], P. Mutton[3], and M. Soodi[4]

heat affected zone (HAZ) of the parent rail is scarce in the open literature. The formation of hard and simultaneously brittle phases in the HAZ is expected to increase the susceptibility to cracking under cyclic, dynamic or high impact loading conditions. In addition, the effects of carbon dilution from the higher carbon substrate on the mechanical and microstructural characteristics of laser cladded deposits, which has been investigated in this paper, is important in controlling the quality and preserving the chemical composition and properties of the laser deposits.

Evaluation of the mechanical performance of the rail steels after cladding plays a vital role in the development of future rail maintenance strategies. Therefore, in this current work, these fundamental issues will be investigated by examining material property data and correlating them to the microstructures of the cladding material and the rail steel substrate.

Furthermore, the proposed heat treatment regime in this paper, which hinders the formation of martensite in HAZ of laser cladded rails, should facilitate utilisation of laser cladding technology in railway applications.

The development of a heat treatment regime to prevent martensite in the HAZ by only altering preheating conditions and its effects on the characteristics of the laser cladded rails are studied in this paper. The preheating conditions were varied by altering the length which was preheated and over which the cladding was then applied. Furthermore, results of the study revealed the influence of diluted carbon from a high carbon rail upon a low carbon laser cladding deposit.

2. MATERIALS AND METHODS

A premium rail grade produced by Nippon Steel Sumitomo Metals Corporation (NSSMC) was selected as the rail substrate. This grade exhibits higher strength and is more wear resistant compared to the head hardened rail grade described in AS 1085.1-2002 [8]. The rail grade selected for the trial complies the requirements outlined in EN 13674-1 for the R400HT grade [9]. Details of the actual composition and that specified for R400HT grade are summarised in Table 1a.

The depositing material was selected to be the 410L stainless steel (Table 1b) with average particle diameter of 150 µm due to its greater compatibility with the laser cladding process, excellent protection to corrosion and abrasion, and reasonable strength and toughness [10-12]. The dimensions over which the cladding was applied were chosen to simulate the rail repair with full constraint and a representative heat sink during a laser cladding deposition. The deposition length using laser cladding was chosen to be 400 mm on a 600-mm long rail. This would allow the critical parts of the deposition, such as the transient state condition at the start and end of the cladding layer and the steady state condition in the middle of the rail sample, to be investigated. Rust and contaminants were removed by grit-blasting before laser cladding.

	Elements in weight percent (wt.%)										
Identification	**C**	**Si**	**Mn**	**P**	**S**	**Cr**	**Ni**	**Mo**	**V**	**Nb**	**Al**
Rail material	0.93	0.28	0.95	0.018	0.014	0.20	<0.01	<0.01	<0.01	<0.01	<0.005
R400HT (*)	0.88-1.07	0.18-0.62	0.95-1.35	0.025 (max)	0.025 (max)	≤0.30	N.S	N.S	0.030 (max)	N.S	0.004

(*) European Committee for Standardization (CEN), EN13674-1:2011 Railway Applications-Track-Rail-Part 1: Vignole railway rails 46kg/m and above.

Table 1a: Chemical compositions of the substrate material (N.S = Not significant).

Materials	**Fe**	**C**	**Mn**	**Si**	**S**	**P**	**Ni**	**Cr**	**Mo**	**Cu**	**V**	**Nb**	**Ti**	**Al**
410L	Bal	0.01	0.51	0.47	0.01	0.01	0.08	12.7	0.01	0.05	0.01	0.02	<0.01	0.01

Table 1b: Chemical compositions of the depositing materials.

2.1 Laser Cladding

The laser cladding process is illustrated schematically in Fig. 1. Laser cladding was carried out with a coaxial head laser comprising of 4 kW IPG fibre laser gun and a Sultzer-Metco twin-10 powder feeder. The laser head was controlled by a Motoman XRC SK 16X 6-axis CNC unit. The laser beam was optically modified to deliver a concentrated circular laser spot of 5 mm on the rail surface. The actual processing parameters are propriety information; and kept constant throughout all the experiments in the current study. Shielding gas of 50% Argon and 50% Helium around the laser beam was used to avoid oxidation during the process.

Effects of preheating and carbon dilution on material characteristics of laser-cladded hypereutectoid rail steels

Q. Lai[1], T. Roy[1], R. Abrahams[1], W. Yan[1], A. Paradowska[2], C. Qiu[3], P. Mutton[3], and M. Soodi[4]

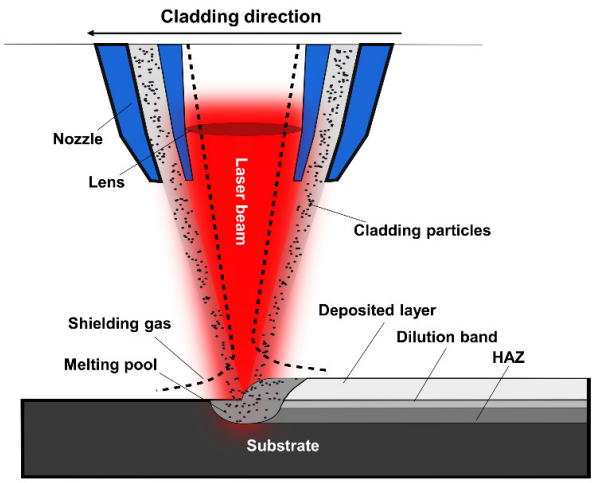

Figure 1: Schematic diagram of laser cladding process

Cladding direction was chosen in the rail longitudinal direction and all other laser cladding parameters were kept constant. Two rail directions were shown in Fig. 2, i.e. along the rail (longitudinal direction) and across the rail (transverse direction).

Preheating at 350 °C was carried out using a conventional manual oxy torch. The full rail head was heated with three thermocouples located at the start, middle, and end of the cladded area to monitor the uniformity of heating. When the preheating temperature of 350 °C was achieved across the specimen, the cladding process was then started. The sample identification and description are summarised in Table 2.

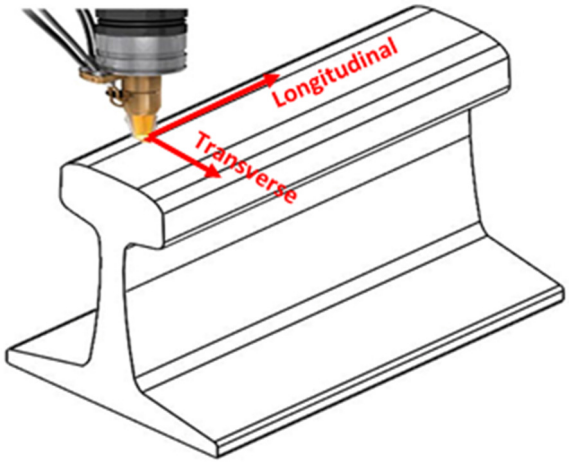

Figure 2: Schematic of laser cladded rail. Rail directions are shown in red.

2.2 Sample Characterisation

Specimens were characterised for microstructure and hardness distribution. Optical microscopy with image analysis was used for microstructure observation. A Kalling's no. 2 (5 g $CuCl_2$, 100 ml HCl and 100 ml ethanol) was used to reveal the microstructure of the clad material and the HAZ. Microhardness measurements were taken using a Struers A300 Duramin hardness tester and a test load of 5 kg-f. These measurements were taken on through-thickness cross sections to investigate the variation in hardness distribution of the different regions (cladding, HAZ and substrate).

Specimens	Preheating length	Cladding length	No.of deposited layers
Group1-1L	400 mm	400 mm	1
Group1-2L	400 mm	400 mm	2
Group2-1L	600 mm	400 mm	1
Group2-2L	600 mm	400 mm	2

Table 2: Sample identification with different cladding process.

3. RESULTS AND DISCUSSION

3.1 Microstructural characteristics of 410L deposited layers

Overview micrographs of the representative rail-cross sections for each of the four considered specimen groups are presented in Fig. 3 for comparison. Fig. 3(i) shows optical images of Group 1-1L which was cladded using one layer and preheating length of 400 mm. The major phases detected are ferrite and martensite with bright and darker etching colours, respectively. The martensitic microstructure is dominant and encloses tiny ferritic grains, particularly near the top surface of the cladded layer. Density of ferritic grains appeared to be significant near the overlapping regions of the laser-tracks and the top surface and to be minimal as approaching the vicinity of the cladding-substrate interface.

With two layers, the microstructural characteristics of Group 1-2L were significantly changed, as shown in Fig. 3(ii). In the second layer, large elongated ferritic grains, surrounded by small portion of martensite matrix, originated from the interface between the first and second layers and extended to the top surface of the second layer due to the high temperature gradient resulting from the second deposition. Unlike the second layer, dendritic morphology was observed from the first layer-substrate interface to the layers' interface. Typical planar dendritic morphology near both the laser track overlapping regions and the cladding-substrate interface were observed.

Effects of preheating and carbon dilution on material characteristics of laser-cladded hypereutectoid rail steels

Q. Lai[1], T. Roy[1], R. Abrahams[1], W. Yan[1], A. Paradowska[2], C. Qiu[3], P. Mutton[3], and M. Soodi[4]

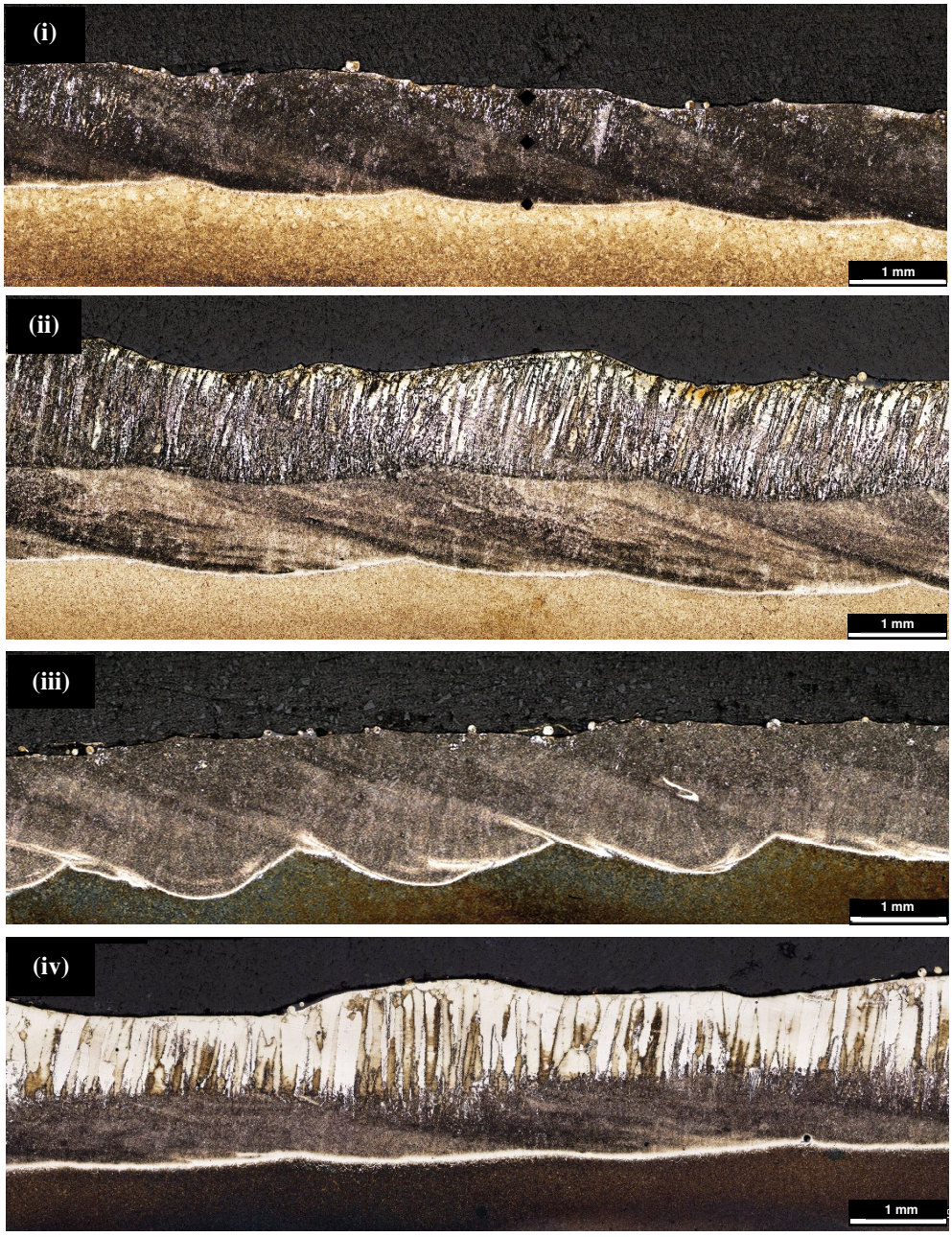

Figure. 3 Optical macrographs of a representative cross section of (i) the Group 1 deposits with one layer and preheating length of 400 mm, (ii) Group 1 deposits with two layers and preheating length of 400 mm, (iii) Group 2 deposits with one layer and preheating length of 600 mm, and (iv) Group 2 deposits with two layers and preheating length of 600 mm.

Micrographs of a typical rail-cross section of the Group 2-1L with one layer and preheating length of 600 mm are shown in Fig. 3(iii). Martensite and ferrite are still the two primary phases in the resulting microstructures of Group 2-1L. However, ferritic grains were not as dense and substantial in size as those in the Group 1-1L and martensitic morphology was occupied dominantly throughout the deposited layer. More homogeneous microstructures were seen across the Group 2 deposits with one and two layers than Group 1.

For Group 2-2L – Fig. 3(iv), the distribution of martensitic morphology was seen to be relatively uniform in the first layer. Like the second layer of the Group 1 deposits, large dendritic ferrite grains developed from the top surface of the first layer. It was also observed that the dendritic ferrite grains in the second layers tend to remelt and join with the preformed ferritic grains at the laser track overlapping regions of the first layer, and leads to the longer elongated ferritic grains in the overlapping regions as shown in Fig. 3(iv).

Q. Lai[1], T. Roy[1], R. Abrahams[1], W. Yan[1], A. Paradowska[2], C. Qiu[3], P. Mutton[3], and M. Soodi[4]

Micrographs of the first layer of Group 2-2L, Fig. 6(a)-(d), show similar microstructural characteristics to those of Group 1-2L.

3.2 Microstructure of 410L deposits' HAZs

The optical micrographs of the heat affected zones (HAZs) in the representative rail-transverse sections from each of the four cladding groups are shown in Fig. 4(i)-(iv). In each group, the four individual micrographs correspond to (a) left gauge corner, (b) right gauge corner, (c) middle section and (d) representative of the longitudinal sections at the starting and finishing ends of the laser tracks, where occurrence of martensite is the most prevalent due to the rapid heat conduction to the neighbouring uncladed surfaces of the laser track pads with the preheating length of 400 mm.

Similar to a previous study conducted by Quan et al [13], typical microstructures consisting of four sub-regions in the HAZ of laser cladded rails, i.e. partially molten zone, coarse-grained HAZ, fine-grained HAZ and spheroidised HAZ were found in the HAZs' microstructures of the four specimen groups.

Contiguous to the partially molten zone, the coarse-grained HAZ was established due to the presence of the high peak temperature beyond Ac3. Increase in the peak temperature would facilitate the growth in grain size. Depending on the rate of cooling, during the cooling stage of the laser deposition, the austenitic grains formed was subjected to different solid-state transformation. Therefore, morphology of the coarse-grained HAZ can be varied, i.e. pearlite, bainite, martensite or tempered martensite.

Martensite was observed to occupy predominantly in the coarse-grained HAZ of both Group 1-1L and Group 1-2L, specifically at the right gauge corners of the rail cross sections and the starting and finishing track ends of the rail-longitudinal sections. This might be attributed to the difference in the rate of cooling experienced in Group 1 and Group 2 cladded rails. In other words, the change in the applied pre-heating lengths influenced the morphology of the coarse-grained HAZ. The Group 1 pre-heating length of 400 mm was insufficient to prevent the martensitic transformation. The resulting effective temperature of 350 °C in the preheated substrate was dissipated rapidly owing to the large surrounding surface area with lower temperature, which led to an effect similar to quenching and hence formation of martensite occurred. The most susceptible regions were at last laser-tracks (right gauge corners), as shown in Fig. 4(i)(c) and Fig. 4(ii)(c), and the starting & finishing ends of laser tracks, as shown in Fig. 4(i)(d) and Fig. 4(ii)(d), where the cooling rate was significant.

On the other hand, in the coarse-grained HAZ of Group 2-1L and Group 2-2L, a microstructural combination of bainite and pearlite was observed. By increasing the pre-heating length to 600 mm in Group 2, the time necessary for the pearlitic and bainitic transformation to begin and end was allowed. The reduced rate of cooling hindered the phenomenon of quenching in not only single deposition, but also double deposition as evident in Fig. 4(iii) and Fig. 4(iv), respectively. Microstructures of the remaining sub-regions in the four specimen groups are relatively analogous. Therefore, due to the occurrence of martensite in the HAZ of the Group 1-1L & Group 1-2L with the preheating length of 400 mm, cracking tendency of these groups is substantially greater than those without.

3.3 Microhardness tests

The effects of variation in the applied length of preheating on the surface hardness of the laser cladded rails was investigated using 5 kgf Vickers indentation on the rail cross sections, i.e. middle, right and left gauge corner sections, of the four groups of specimens. Hardness indentations were performed along vertical traversing through the deposited layers, HAZ and unaffected rail substrate.

Fig. 5(a) shows the vertical microhardness variation of Group 1-1L's cross sections. In the deposited layer, average hardness values of 373 HV, 403HV and 388 HV were determined for the middle, left and right gauge corner sections respectively. Average hardness values were measured to be 403 HV, 399 HV and 635 HV at the middle section, left gauge corner, and right gauge corner of the HAZ, respectively.

Likewise, the vertical microhardness variation of Group 1-2L's cross sections is illustrated in Fig. 9(b). Average hardness values of 323 HV, 373 HV and 340 HV were acquired for middle, left and right gauge corner sections respectively. The average hardness of Group 1-2L's HAZ for middle, left and right gauge corner sections were 352 HV, 360 HV, and 463 HV, respectively.

For Group 2-1L cross sections, the vertical microhardness variation of the cross sections is shown in Fig. 5(c). Average hardness values of 387 HV, 431 HV and 409 HV were respectively obtained for middle, left and right gauge corner sections in the cladding layer. The HAZ's average hardness of Group 2-1L specimens for middle, left and right gauge corner sections respectively were 368 HV, 371 HV, and 378 HV, respectively.

Average hardness values were 279 HV, 269 HV and 292 HV for middle, left and right gauge corner sections of Group 2-2L's cross sections, respectively as illustrated in Fig. 5(d). Whereas, the HAZ's average hardness of Group 2-2L for middle, left and right gauge corner sections were

Q. Lai[1], T. Roy[1], R. Abrahams[1], W. Yan[1], A. Paradowska[2], C. Qiu[3], P. Mutton[3], and M. Soodi[4]

determined to be 385 HV, 389 HV, and 384 HV, respectively.

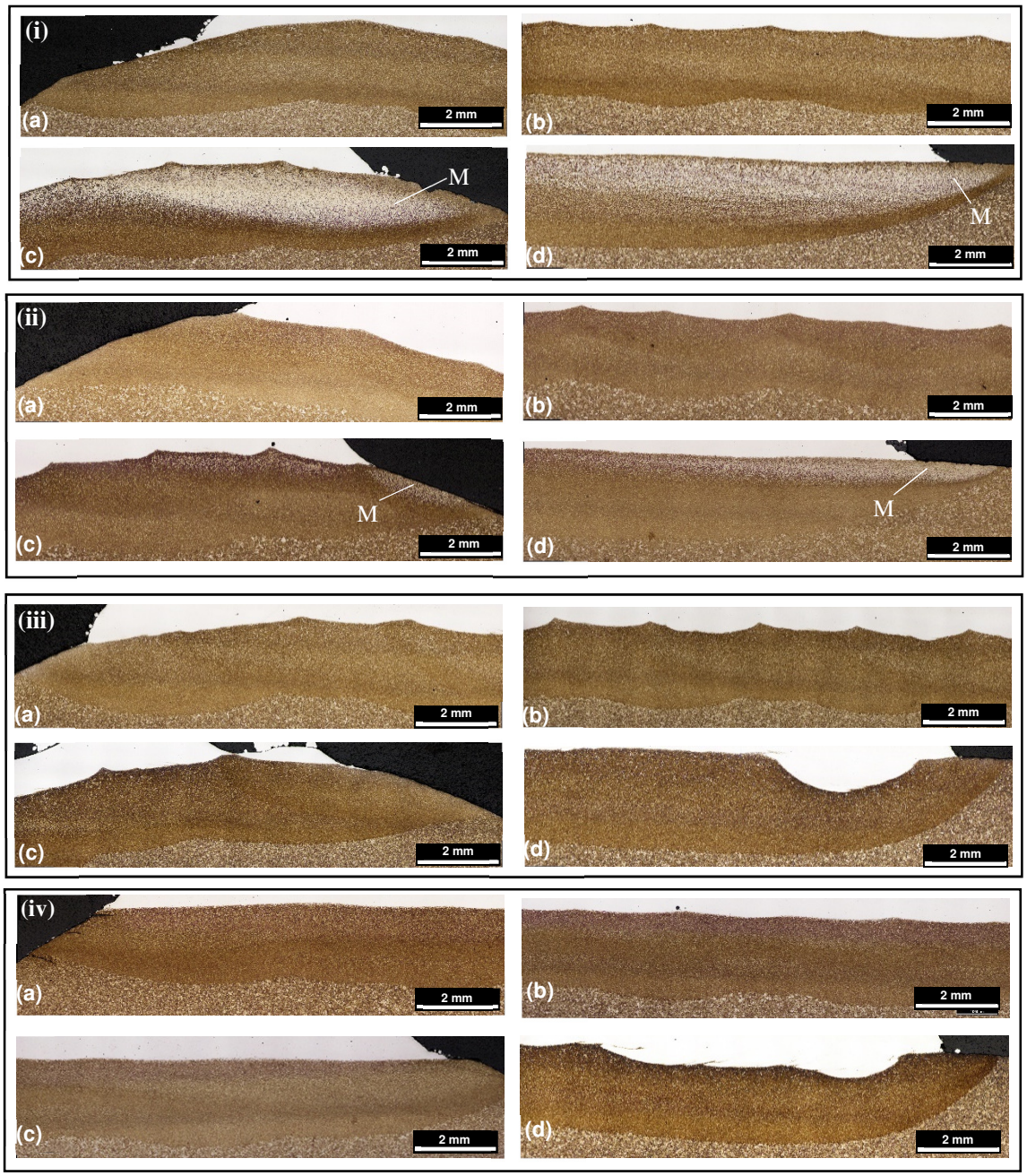

Figure 4 Unaffected rail substrate and corresponding HAZ of a typical rail-transverse sections at (a) left gauge corner, (b) middle section, (c) right gauge corner and (d) representative of the longitudinal sections for (i) Group 1-1L, (ii) Group 1-2L, (iii) Group 2-1L & (iv) Group 2-2L. Martensitic morphology (M=martensite) with white etching colour were detected in (c) and (d) of the (i) Group 1-1L and (ii) Group 1-2L.

An increase in hardness at the right gauge corners, where the last laser tracks located, of Group 1-1L and Group 1-2L was correlated to the formation of martensite in the fine-grained HAZ, as shown in Fig. 5(i)(c) and Fig. 5(ii)(c). The investigation by Quan et al. [14] also showed higher average hardness values at the last laser tracks for preheating length of 400 mm, regardless of cladding directions, and the addition of PWHT provided relatively uniform average hardness across the laser deposits' HAZ, but the HAZ's average hardness values are greater than that of parent rail with the presence of tempered martensite. However, in the current study, the application of a longer preheating length leads to a small variation in the HAZ's average hardness across the railheads and the values of the HAZ's

Q. Lai[1], T. Roy[1], R. Abrahams[1], W. Yan[1], A. Paradowska[2], C. Qiu[3], P. Mutton[3], and M. Soodi[4]

average hardness being closer to the parent rails due to the avoidance of martensite formation in the HAZ.

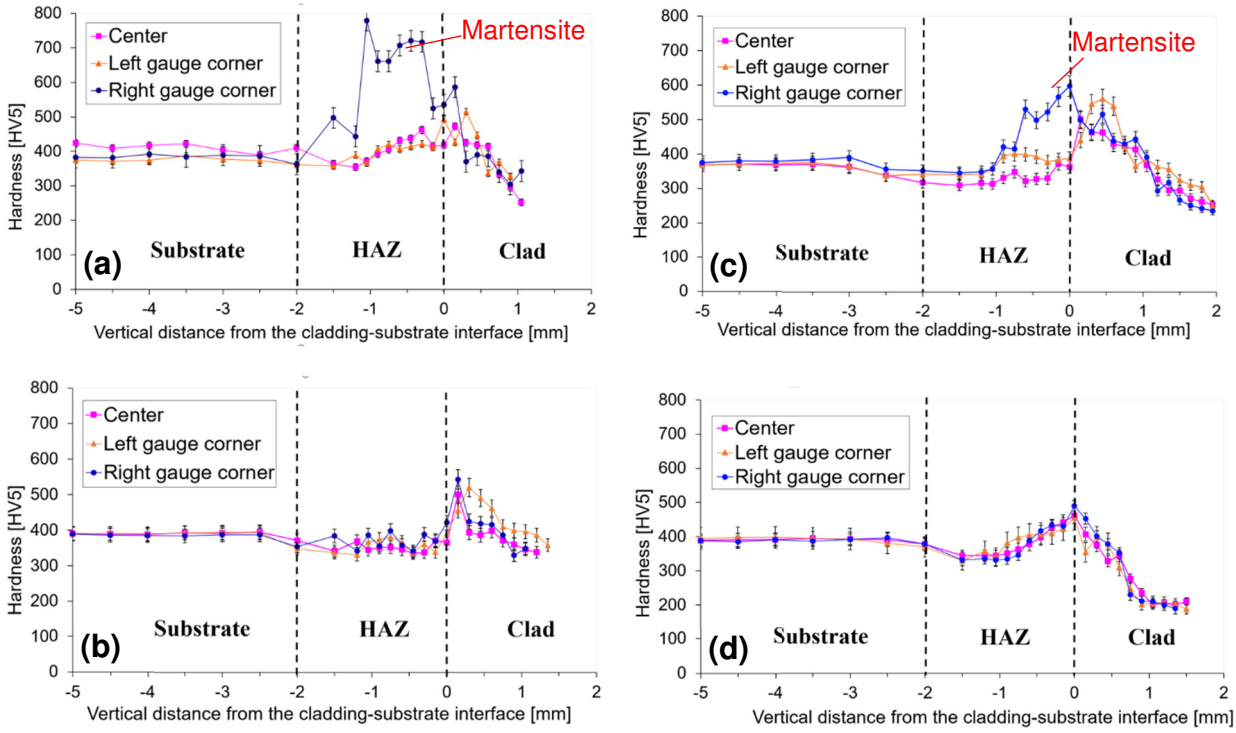

Figure 5 Vertical hardness distributions in the laser deposited rails (a) Group 1-1L, (b) Group 1-2L, (c) Group 2-1L and (d) Group 2-2L.

4. CONCLUSIONS

The presented investigations established the importance and significance of applying an appropriate preheating to multi-layer laser deposition on hypereutectoid rails. According to the study, the following can be concluded:

- Formation of martensite in the HAZs of laser cladded hypereutectoid rails, which is known for its adverse impacts, was eliminated for both single and double deposition by increasing the length of preheating from 400 mm to 600 mm. The increase in preheating length retards the rate of cooling and, therefore, hinders the phenomenon of quenching as the laser source traverses along the cladded rail.

- For the cladded layers undergone either single or double-layer laser deposition, application of a longer preheating length of 600 mm resulted in a more homogeneous microstructure in the cladded layers. In absence of preheating, dendritic morphology was found to dominantly occupy the deposits' microstructure.

- Dilution of carbon in the laser deposition of the 410L stainless steel on hypereutectoid rails was observed to be substantial. Dilution band was estimated to be approximately equal to the thickness of the first deposited layers. Martensitic morphology was found in the dilution band as a result of the increase in carbon content.

5. ACKNOWLEDGMENT

This work was supported by the Australian Research Council (ARC), Hardchrome Engineering, the Welding Technology Institute of Australia (WTIA), the Australian Nuclear Science, and Technology Organisation (ANSTO) - ARC Linkage project [grant number LP140100810]. The authors would like to acknowledge the invaluable assistance received from Mr Andrew Dugan – the general manager of Hardchrome Engineering and the Institute of Railway Technology (IRT).

6. REFERENCES

[1] R. DiMelfi, P. Sanders, B. Hunter, J. Eastman, K. Sawley, K. Leong, J. Kramer, Mitigation of subsurface crack propagation in railroad rails by

Effects of preheating and carbon dilution on material characteristics of laser-cladded hypereutectoid rail steels

Q. Lai[1], T. Roy[1], R. Abrahams[1], W. Yan[1], A. Paradowska[2], C. Qiu[3], P. Mutton[3], and M. Soodi[4]

laser surface modification, Surface and Coatings Technology 106(1) (1998) 30-43.
[2] S. Aldajah, O.O. Ajayi, G.R. Fenske, S. Kumar, Investigation of top of rail lubrication and laser glazing for improved railroad energy efficiency, Journal of Tribology 125(3) (2003) 643-648.
[3] S. Shariff, T. Pal, G. Padmanabham, S. Joshi, Sliding wear behaviour of laser surface modified pearlitic rail steel, Surface Engineering 26(3) (2010) 199-208.
[4] S. Niederhauser, B. Karlsson, Fatigue behaviour of Co–Cr laser cladded steel plates for railway applications, Wear 258(7) (2005) 1156-1164.
[5] J.W. Ringsberg, A. Skyttebol, B.L. Josefson, Investigation of the rolling contact fatigue resistance of laser cladded twin-disc specimens: FE simulation of laser cladding, grinding and a twin-disc test, International Journal of Fatigue 27(6) (2005) 702-714.
[6] F. Franklin, G.-J. Weeda, A. Kapoor, E. Hiensch, Rolling contact fatigue and wear behaviour of the Infrastar two-material rail, Wear 258(7) (2005) 1048-1054.
[7] M. Hiensch, P.-O. Larsson, O. Nilsson, D. Levy, A. Kapoor, F. Franklin, J. Nielsen, J.W. Ringsberg, B.L. Josefson, Two-material rail development: field test results regarding rolling contact fatigue and squeal noise behaviour, Wear 258(7) (2005) 964-972.
[8] A. Standard, Railway Track Materials, Part 1: Steel Rails. AS1085. 1-2002 (2002).
[9] T. EN, 13674-1): Railway applications–track–rail–part 1: Vignole railway rails 46 kg/m and above, Brussels, 2011.
[10] B.V. Krishna, A. Bandyopadhyay, Surface modification of AISI 410 stainless steel using laser engineered net shaping (LENS TM), Materials & Design 30(5) (2009) 1490-1496.
[11] P. Krakhmalev, I. Yadroitsava, G. Fredriksson, I. Yadroitsev, In situ heat treatment in selective laser melted martensitic AISI 420 stainless steels, Materials & Design 87 (2015) 380-385.
[12] Y. Zhang, G. Yu, X. He, W. Ning, C. Zheng, Numerical and experimental investigation of multilayer SS410 thin wall built by laser direct metal deposition, Journal of Materials Processing Technology 212(1) (2012) 106-112.
[13] D. Housed, Welding of Railroad Rails—A Literature and Industry Survey', Rail Steels: Developments, processing, and use 644 (1978) 118.
[14] Q. Lai, R. Abrahams, W. Yan, C. Qiu, P. Mutton, A. Paradowska, M. Soodi, Investigation of a novel functionally graded material for the repair of premium hypereutectoid rails using laser cladding technology, Composites Part B: Engineering (2017).